Journal of Inorganic and Organometallic Polymers and Materials (2020) 30:4043–4052
https://doi.org/10.1007/s10904-020-01550-5

Incorporation of CuO/TiO_2 Nanocomposite into MOF-5 for Enhanced Oxygen Evolution Reaction (OER) and Photodegradation of Organic Dyes

Abdul Jabbar[1] · Muhammad Fiaz[1] · Sonia Rani[1] · Muhammad Naeem Ashiq[1] · Muhammad Athar[1]

Received: 18 March 2020 / Revised: 14 April 2020 / Accepted: 16 April 2020 / Published online: 29 April 2020

Abstract

In this reported article, a highly efficient, stable and low cost CuO/TiO_2@MOF-5 composite has been synthesized by in-situ incorporation of pre-synthesized precursors into MOF-5. The formation of synthesized samples has been confirmed by Powder X-ray diffraction (PXRD), Scanning electron microscopy (SEM) images, Energy dispersive X-ray (EDX) images and Ultraviolet visible spectrophotometry. The synthesized samples are found efficient for photoelectrochemical oxygen evolution reaction (OER) and photodegradation of organic dyes (methylene blue/methyl orange). It has been observed that CuO/TiO_2@MOF-5 shows lowest onset potential, highest current density and better OER activity as compared to some of previously reported Cu-based working electrodes. It required only 263 mV overpotential to deliver the benchmark 10 mA cm^{-2} current density. In the same way, CuO/TiO_2@MOF-5/NF exhibits maximum ability to degrade methylene blue and methyl orange as compared to all other samples.

Graphic Abstract

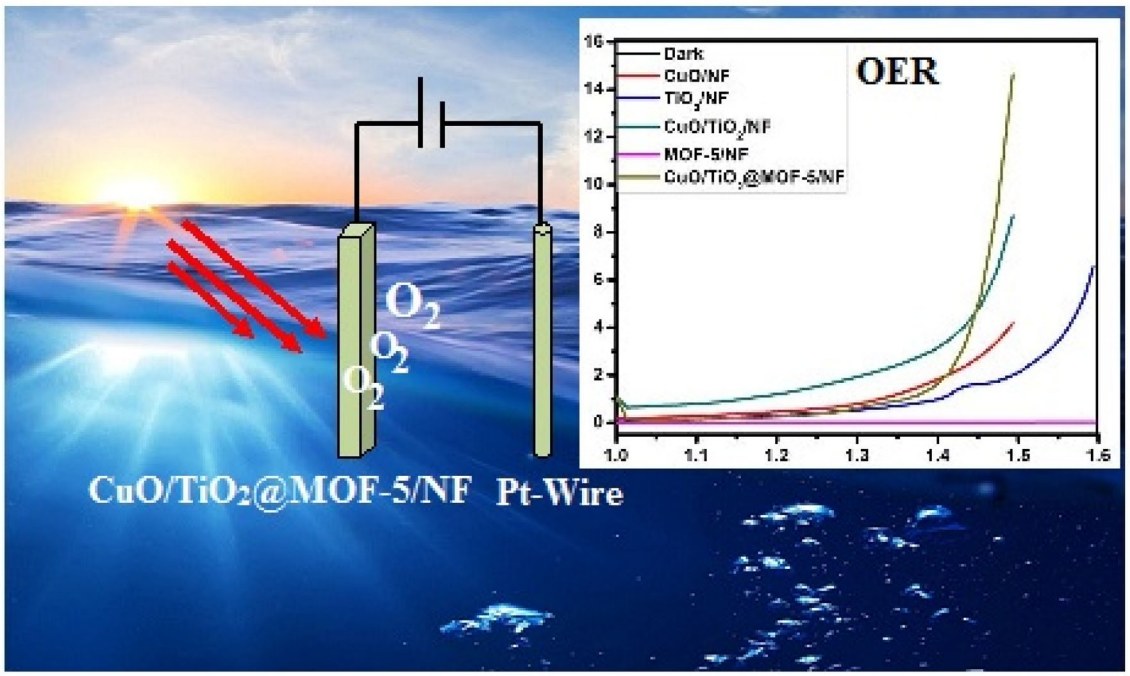

Keywords Metal–organic frameworks · Nanoparticles · Oxygen Evolution Reaction (OER) · Photodegradation · Organic dye

Extended author information available on the last page of the article

1 Introduction

With the increasing demands of energy and rapid consumption of fossil fuels, search of alternate and renewable energy sources has attracted a great research attention. Amongst different alternate energy sources, hydrogen represents itself as a most promising alternate and renewable energy source [1]. The production of hydrogen through photoelectrochemical water splitting has been widely used as one of the most promising way to produce clean and renewable H_2 fuel [2]. Water splitting consists of two half reactions: Oxygen evolution reaction (OER) at photoanode and hydrogen evolution reaction (HER) at photocathode. Both these reactions are kinetically sluggish because they required a lot of overpotential [3].

Oxygen evolution reaction (OER) is kinetically more sluggish as compared to HER because of the four-electron coupled reactions [4]. Recently, the most efficient OER catalysts are based on noble metals (Ir or Ru) but due to their scarcity and high cost, they cannot be used at commercial level [5]. So, a lot of research attention has been focused on the development of low cost, efficient and non-noble metal based OER catalysts such as transition metal oxides, phosphides, sulphides and selenides [6–9].

MOFs (metal-organic frameworks) are a class of organic and inorganic hybrid porous materials, which have been generating a rapid expansion and development in many potential applications such as gas storage, CO_2 capture, separation, catalysis etc. This is due to easily tailored, modified and diverse structures of MOFs [10–15]. Now a day, MOFs have been emerged as a new class of OER catalysts because of their unique properties [16]. But, efficient MOF as an OER catalyst has not been well explored due to sluggish kinetics and instability. Therefore, different strategies have been proposed to enhance the OER activity of MOFs and one of them is the incorporation of pre-synthesized 3d transition metal oxide nanoparticles into MOFs to make an efficient MOF-based OER catalyst. Out of various MOFs, MOF-5 has been reported as an efficient photocatalyst [17].

Amongst 3d-transition metal oxide nanoparticles, TiO_2 and CuO nanoparticles have been widely studied due to their appreciative chemical and physical properties, non-toxicity, chemical stability and low cost [18–20]. So, composite formation of CuO with TiO_2 as TiO_2/CuO nanocomposite has been reported as an efficient photocatalyst for water splitting and photodegradation of many organic pollutants [21].

In this reported research work TiO_2, CuO nanoparticles and their nanocomposite TiO_2/CuO were synthesized and successfully incorporated into MOF-5 by in-situ incorporation of pre-synthesized precursors into MOF-5. Further they were used for photoelectrochemical studies towards oxygen evolution reaction (OER) and photodegradation of methylene blue and methyl orange. Amongst, CuO/TiO_2@MOF-5 exhibits excellent catalytic activity towards both OER and photodegradation of organic dyes.

2 Experimental Work

2.1 Chemicals

Zinc (II) chloride ($ZnCl_2$, Merck, 98%); Titanium (IV) chloride ($TiCl_4$, Merck, 99%); Copper (II) chloride dihydrate ($CuCl_2{\cdot}2H_2O$, Merck, 99.99%); Terephthalic acid (1,4-H_2BDC, Merck, 98%); N,N-dimethylformamide (DMF, Merck, 99.8%); Sulphuric acid (H_2SO_4,Merck, 98%); Sodium hydroxide (NaOH, 97%), Potassium hydroxide (KOH, Merck, 85%); Ammonium hydroxide (NH_4OH, Merck, 32%); Acetic acid (CH_3COOH, Merck, 99%).

3 Preparation of CuO Nanoparticles

Nanoparticles of CuO were synthesized by using sol-gel method as reported in the literature [22]. 0.2 M aqueous solution of $CuCl_2{\cdot}2H_2O$ was prepared by dissolving 3.40 g of $CuCl_2.2H_2O$ in 100 mL de-ionized water. 1 mL of glacial acetic acid was added to above solution and heated the whole mixture at 100 °C under constant stirring. Then 8M NaOH was added drop-wise until pH reached 7. Black precipitates were obtained, which were separated by centrifugation, washed with de-ionized water and dried at 50 °C for 24 h.

3.1 Preparation of TiO_2 Nanoparticles

TiO_2 nanoparticles were synthesized by hydrolysis of $TiCl_4$ as reported previously [23]. In brief, 1 mL of $TiCl_4$ was added to 10% sulphuric acid at 0 °C with continuous stirring for 30 min. A gray solution was formed. It was then heated upto 60 °C to form a clear solution. Then, NH_4OH was added drop-wise to above solution until pH reached 7 and a white solution formed. At last, the white solution was cooled to room temperature and gelled for 12 h. After that, white powder of hydrousTiO_2 was formed, which was separated by centrifugation, washed with de-ionized water and dried in air. The dried precipitates were calcinated at 400 °C to get off-white precipitates of TiO_2 nanoparticles.

3.2 Preparation of CuO/ TiO_2 Nanocomposite

The CuO/TiO_2 nanocomposite was synthesized by precipitation method. 6 mL of concentrated sulphuric acid was added to 10 mL of distilled water and cooled to 0 °C. Then,

2.88 mL of $TiCl_4$ and 3.10 g of $CuCl_2{\cdot}2H_2O$ were added in above solution and temperature was maintained at 35 °C. Afterthat, 5M NaOH was added drop-wise until black precipitates were obtained, which were separated by centrifugation, washed with distilled water and dried in air. The dried precipitates were calcinated at 400 °C for 3 h to get CuO/TiO_2nanocomposite.

3.3 Preparation of MOF-5

For the synthesis of MOF-5, 1.410 g of $ZnCl_2$ was dissolved in 20 mL of DMF by sonication for 1 h. In another beaker, 1.295 g of 1, 4-BDC was dissolved in 20 mL DMF and added dropwise to the above mixture under continuous stirring. Then, whole mixture was stirred for 12 h. White precipitates were obtained, separated by centrifugation, washed with de-ionized water/DMF and dried at 60°C for 6 h. Finally, the dried precipitates were ground and stored for further process.

3.4 Incorporation of CuO/TiO_2intoMOF-5

CuO/TiO_2@MOF-5 composite was synthesized by in-situ incorporation of pre-synthesized CuO/TiO_2 composite into MOF-5 at room temperature. Typically, 1.410 g of $ZnCl_2$ and 0.020 g of CuO/TiO_2 composite were dissolved in 20 mL of DMF by sonication for 1 h. In another beaker, 1.295 g of 1, 4-BDC was dissolved in 20 mL DMF and added dropwise to the above mixture under continuous stirring. Then, whole mixture was stirred for 12 h. Light green precipitates were obtained, separated by centrifugation, washed with de-ionized water/DMF and dried at 60°C for 6 h. Finally, the dried precipitates were ground and stored for further process.

3.5 Measurement of Dye Degradation by Prepared Samples

1×10^{-4} M dye solutions were prepared by dissolving 0.035 g of methylene blue and 0.033 g of methyl orange in 1.0 L distilled water separately. The λ_{max} value of methylene blue and methyl orange were measured by UV-visible spectrophotometer. λ_{max} of methylene blue and methyl orange were measured as 663.5 nm and 465.6 nm respectively.

0.2 g of Sample was mixed in the 100 mL dye solution with maximum absorbance and kept in dark with constant stirring for 30 min. 5 mL of sample was taken and to remove the solid particles centrifuged and its absorbance was measured by spectrophotometer. The remaining solution was kept in a closed reactor under UV light. UV–Vis absorbance of the solution was measured after every 10 min interval by taking out 5 mL sample from the stock.

3.6 Preparation of Working Electrodes

The working electrodes were prepared on a piece (1 cm × 1 cm) of nickel foam. The piece of Ni-foam was cleaned by washing with acetone and distilled water, dried at 50° for 2 h. The slurry of synthesized samples was prepared by adding 0.01 g of sample in 2 mL distilled water and sonicated for 30 min to form uniform slurry. Then, slurry was pasted uniformly on a pre-cleaned piece of Ni-foam and dried in an oven at 50° for 6 h.

3.7 Electrochemical Studies for Oxygen Evaluation Reaction (OER)

Electrochemical studies were performed by using a common three electrode set-up containing Ag/AgCl as reference electrode, Pt-wire as counter electrode and catalyst@ Ni-foam as working electrode in 1 M $KOH_{(aq)}$ electrolyte. The cyclic voltammetry and linear sweep voltammetry were performed to evaluate the catalytic activity towards OER at $50mVs^{-1}$ and $1mVs^{-1}$, respectively. All the potential data is converted into reversible hydrogen electrode (RHE) by using the following equation [24].

$$E_{RHE} = E_{Ag/AgCl\,/Sat.KCl} + 0.197 + 0.059\,pH. \quad (1)$$

Overpotential (η) for OER has been calculated from linear sweep voltammetry (LSV) by using following equation.

$$\eta = E_{RHE} - 1.23 \quad (2)$$

3.8 Characterizations

Powder X-ray diffraction patterns (P-XRD) of all the synthesized samples were obtained by using Shimadzu X-ray diffractometer with Cu-Kα radiation (λ = 0.15406 nm) in 2θ range 5° to 55°. The morphology and composition of synthesized samples were evaluated through scanning electron microscopy (SEM) images and energy dispersive X-ray (EDX) spectra by using Philips XL30 Environmental SEM attached with an Oxford Instrument Inca 500 Energy Dispersive X-ray Spectrometer (EDX). The optical properties of synthesized samples were measured through Shimadzu UV-2600 spectrophotometer in wavelength range 200–900 nm.

4 Results and Discussion

The PXRD patterns of all synthesized samples are represented in Fig. 1. In the PXRD pattern of $TiO_2$and CuO all the diffraction peaks are in well agreement with the

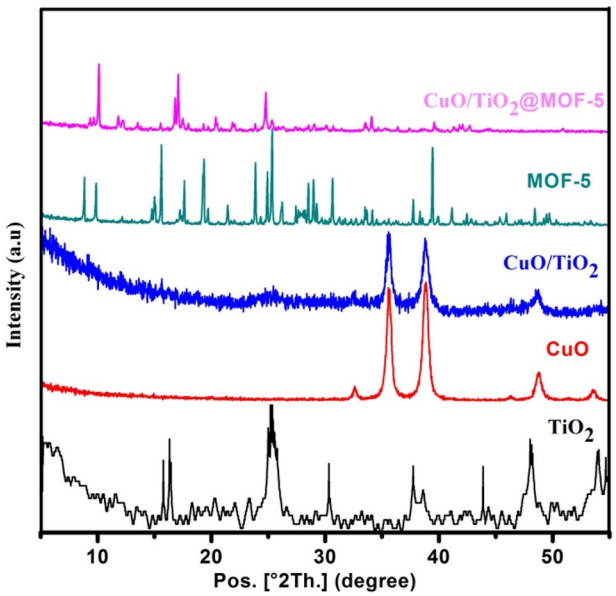

Fig. 1 PXRD patterns of TiO2, CuO, CuO/TiO_2, MOF-5 and CuO/TiO_2@MOF-5

reported pattern of TiO_2 and CuO, respectively. In the same way, diffraction pattern of MOF-5 is in good agreement with reported pattern of MOF-5. It indicates successful synthesis of crystalline Zn-based MOF MOF-5, $TiO_2$and CuO nanoparticles.

PXRD pattern of CuO/TiO_2 composite contains diffraction peaks indexed to both CuO and TiO_2 nanoparticles. Diffraction peak at 2θ about 25.20° indexed to TiO_2 anatase structure and matched well with JCPDS card number 21-1272 and diffraction peaks at 2θ about 32.62°, 35.58°,38.87° and 48.74° indexed to CuO. PXRD diffraction pattern of CuO/TiO_2@MOF-5 contains most of diffraction peaks indexed to MOF-5 and some additional peaks are also observed related to CuO/TiO_2composite. However, it is also observed that in PXRD pattern of CuO/TiO_2@MOF-5, the two main diffraction peaks of CuO around 35° to 40° are not more visible because these are overlaid by MOF-5. It shows that MOF-5 maintains its crystalline structure and shows its dominance after the incorporation of CuO/TiO_2 composite.

The morphology of all the synthesized samples is studied by scanning electron microscopy (SEM) images, represented by Fig. 2a—e. SEM images of CuO and TiO_2 show that they have been grown in small irregular particles, which are highly agglomerated, shown by Fig. 2a, b. Figure 2c represents the SEM image of CuO/TiO_2 composite, which shows that it has grown in block shape crystals. While SEM image of MOF-5, Fig. 2d, reveals that MOF-5 has grown in uniform and well distributed rectangular shape crystalline form with smooth surfaces and no agglomeration is observed. Similarly, it can be observed from SEM image of CuO/TiO_2@MOF-5 that it has also grown in rectangular shaped crystalline form with smooth surfaces, represented by Fig. 2e.

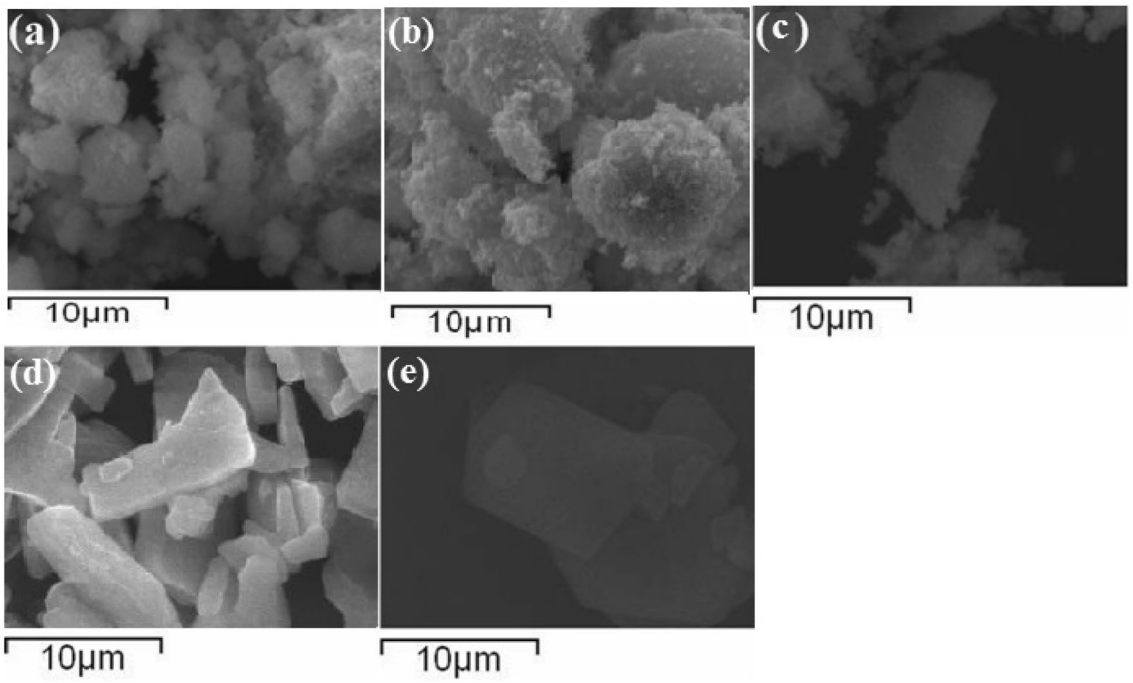

Fig. 2 SEM images of **a** CuO; **b** TiO_2; **c** CuO/TiO_2 composite; **d** MOF-5 and **e** CuO/TiO_2@MOF-5.

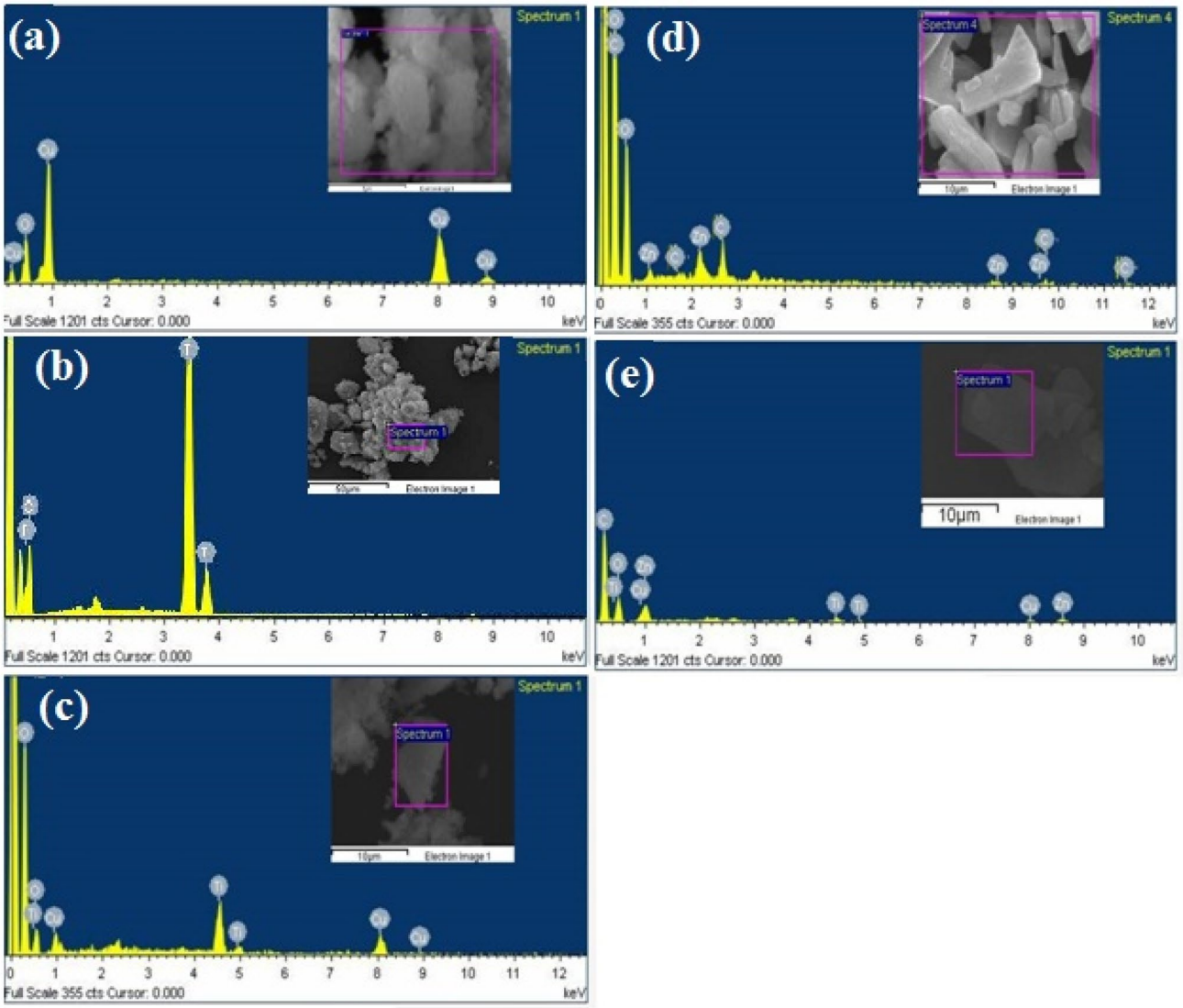

Fig. 3 SEM based EDX spectra of **a** CuO; **b** TiO_2; **c** CuO/TiO_2 composite; **d** MOF-5 and **e** CuO/TiO_2@MOF-5; Inset are the SEM images for EDX analysis

The composition of all the synthesized samples has been studied by SEM based EDX analysis, represented by Fig. 3(a-e). Figure 3a represents the EDX spectrum of CuO, it shows that it contains the basic peaks of Cu and O (from CuO nanoparticles) and no other peak is observed. In the same way, EDX spectrum of TiO_2 contains basic diffraction peaks of Ti and O as shown in Fig. 3b. Similarly, EDX spectrum of CuO/TiO_2 reveals that it contains peaks index to both CuO and TiO_2nanoparticles, represented by Fig. 3c. It can be seen from the EDX spectrum of MOF-5 that it contains diffraction peaks related to Zn, C and O and the EDX spectrum of CuO/TiO_2@MOF-5 shows that it contains additional peaks for Cu and Ti in addition to peaks of MOF-5. It indicates the successful incorporation of CuO/TiO_2 composite into MOF-5, shown by Fig. 3d and e respectively. In all these EDX spectra, no extra peak for impurity is observed which indicates high purity and single phase formation of these samples.

The optical properties measured by UV-Vis Spectrophotometry, Fig. 4a represent the UV-Vis spectra of all the synthesized samples. It can be observed from UV-Vis spectra of MOF-5 that it shows maximum absorption in UV-region with λ_{max} at 256 nm and shows no absorption in visible region. However, after the incorporation of CuO/TiO_2 composite into MOF-5, CuO/TiO_2@MOF-5 shows a shift towards lower wavelength in UV-region with λ_{max} at 230 nm and a new absorption peak is also observed in the visible region with λ_{max} at 697 nm. Tauc plot is derived from UV-Vis spectra of the synthesized samples to study the band gap, represented by Fig. 4b. The band gap of all these

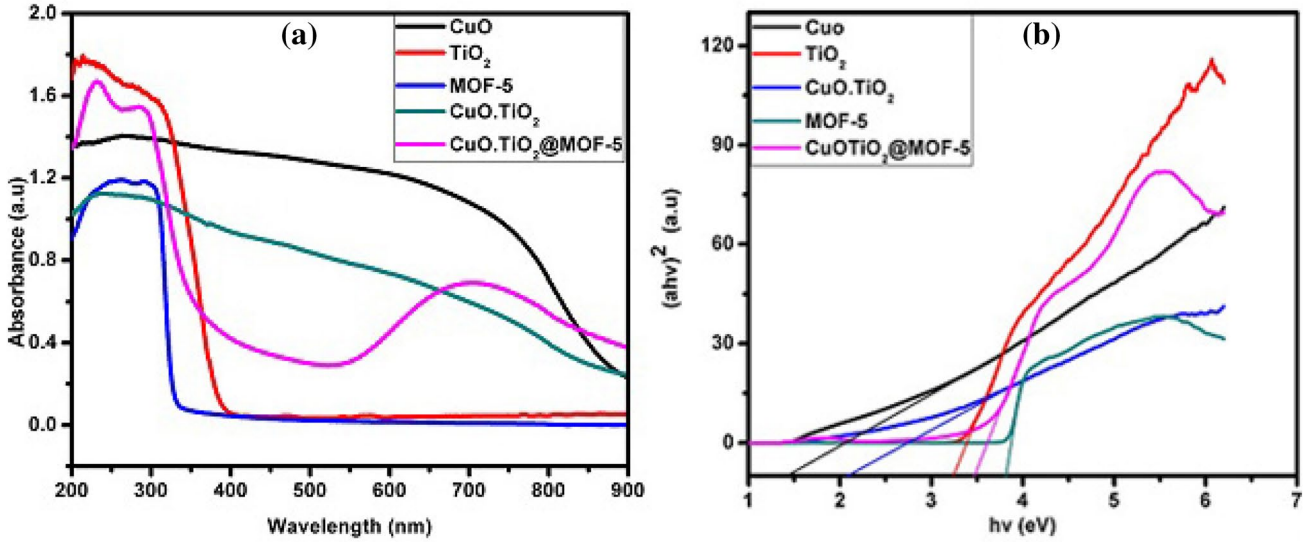

Fig. 4 **a** and **b** UV-Vis spectra and Tauc plot of CuO, TiO_2, CuO/TiO_2, MOF-5 and CuO/TiO_2@MOF-5 composite, respectively

samples has been calculated from Tauc plot by extrapolating the absorption edges by using following equation [25].

$$\alpha h\nu = \left(h\nu - E_g\right)^{0.5} \tag{3}$$

where α = absorption coefficient, h = Planck's constant, ν = wavenumber.

The band gap of CuO and TiO_2 are 1.44 and 3.23 eV, respectively while their composite CuO/TiO_2 has intermediate band gap of 2.10 eV. Bare MOF-5 has band gap of 3.78 eV and after the incorporation of CuO/TiO_2 nanocomposite, band gap of CuO/TiO_2@MOF-5 is 3.45 eV. It indicates that incorporation of CuO/TiO_2 nanocomposite into MOF-5 has shifted the band gap towards more visible region due to synergistic effect and hetero-junction formation between CuO/TiO_2 and central metallic cluster $[Zn_4O]^{6+}$ of MOF-5, which increased the absorption of visible light, reduced the electron-hole pair recombination and enhanced the photocatalytic activity.

4.1 Photoelectrochemical studies towards OER

All the synthesized samples have been used for photoelectrochemical studies towards oxygen evolution reaction (OER) via water splitting, both in the presence of dark and visible light. OER measurements have been observed by cyclic voltammetry (CV) and linear sweep voltammetry (LSV) at $50 mVs^{-1}$ and $1 mVs^{-1}$ scan rate, respectively. The CV curves of all the synthesized samples are shown in Fig. 5a within potential range of 1.0 to 2.0 V vs. RHE. It is observed from CV curves that all the synthesized samples show zero current density in dark. It can be seen from the CV curves that MOF-5/NF does not show any OER activity and generates almost zero current density, both in dark as well as in the presence of visible light. However, after the incorporation of CuO/TiO_2 nanocomposite into MOF-5 and in the presence of visible light prominent increase of current density was observed due to OER activity. The CV curves reveal that among all the synthesized samples, CuO/TiO_2@MOF-5/NF shows lowest onset potential and maximum current density as compared to all other samples. It indicates that CuO/TiO_2@MOF-5/NF shows better OER activity as compared to all other samples due to hetro-junction formation between CuO/TiO_2 and MOF-5.

Further, photoelectrochemical activity of synthesized samples towards OER is evaluated by linear sweep voltammetry (LSV) measurements, represented by Fig. 6b. Like CV, LSV curves also evaluated that MOF-5/NF does not show any OER activity. For comparative studied, overpotential required to achieve 2 mA cm^{-2} current density is considered. It is observed that CuO/TiO_2@MOF-5 needs only 153 mV overpotential to reach the current density of 2 mA cm^{-2}as compared to all other synthesized samples CuO/NF (η_2 = 183 mV), TiO_2/NF(η_2 = 273 mV) and CuO/TiO_2/NF(η_2 = 163 mV), represented by Fig. 6c.It can also be observed that among all synthesized samples only CuO/TiO_2@MOF-5/NF delivers the benchmark of 10 mA cm^{-2} current density at just 263 mV overpotential, which is superior than some of the previously reported Cu-based OER catalysts as shown in Table 1. It reveals that CuO/TiO_2@MOF-5/NF shows lowest onset potential, lowest overpotential to deliver 2 mA cm^{-2} current density and better OER activity as compared to all other synthesized samples. Further, the excellent OER activity of CuO/TiO_2@MOF-5/NF is understand by Tafel plot

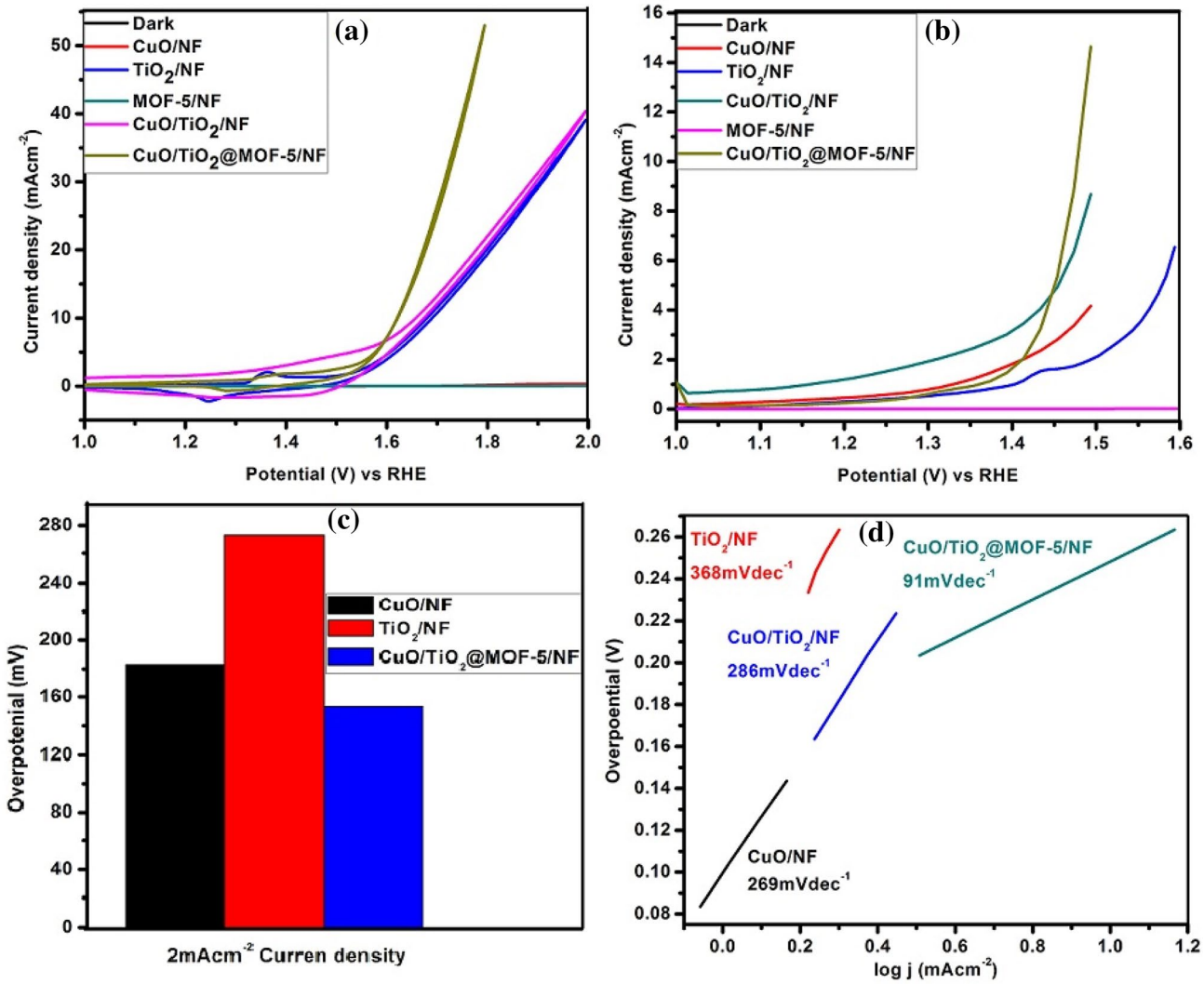

Fig. 5 **a** CV curves and **b** LSV curves of CuO/NF, TiO_2/NF, CuO/TiO_2/NF and CuO/TiO_2@MOF-5/NF; **c** overpotential required to deliver 2 mA cm^{-2}; **d** Tafel plot of CuO/NF, TiO_2/NF, CuO/TiO_2/NF and CuO/TiO_2@MOF-5/NF

derived from LSV curve, represented by Fig. 6d. Tafel plot is derived from LSV curve by using equation [26];

$$\eta = a + b \log j \quad (4)$$

where η = overpotential, j = current density and b = Tafel slope.

The calculated Tafel slope of CuO/TiO_2@MOF-5/NF is just 91 mV dec^{-1}, which is lowest as compared to all other synthesized samples CuO/NF (269 mV dec^{-1}), TiO_2 (368 mV dec^{-1}) and CuO/TiO_2 (286 mV dec^{-1}). It indicates thatCuO/TiO_2@MOF-5/NF has faster and better electron transfer as compared to all other synthesized samples, which enhanced its activity as compared to other synthesized samples.

4.2 Photodegradation of Organic dyes

All the synthesized samples have been used for the degradation of methylene blue (MB) and methyl orange (MO) in the presence of visible light. Methylene blue and methyl orange are effectively oxidized by CuO, TiO_2, CuO/TiO_2, MOF-5 and CuO/TiO_2@MOF-5, as shown in Fig. 7. It can be observed from Fig. 7 (a) and (b) that with the passage of time due to degradation of MB and MO, concentration and absorbance are decreased.

Transition metal oxide nanoparticles are considered as active photocatalysts due to their suitable band gap for visible light harvesting but their activities are still less due to rapid electro-hole pair recombination [27, 28]. So, individual

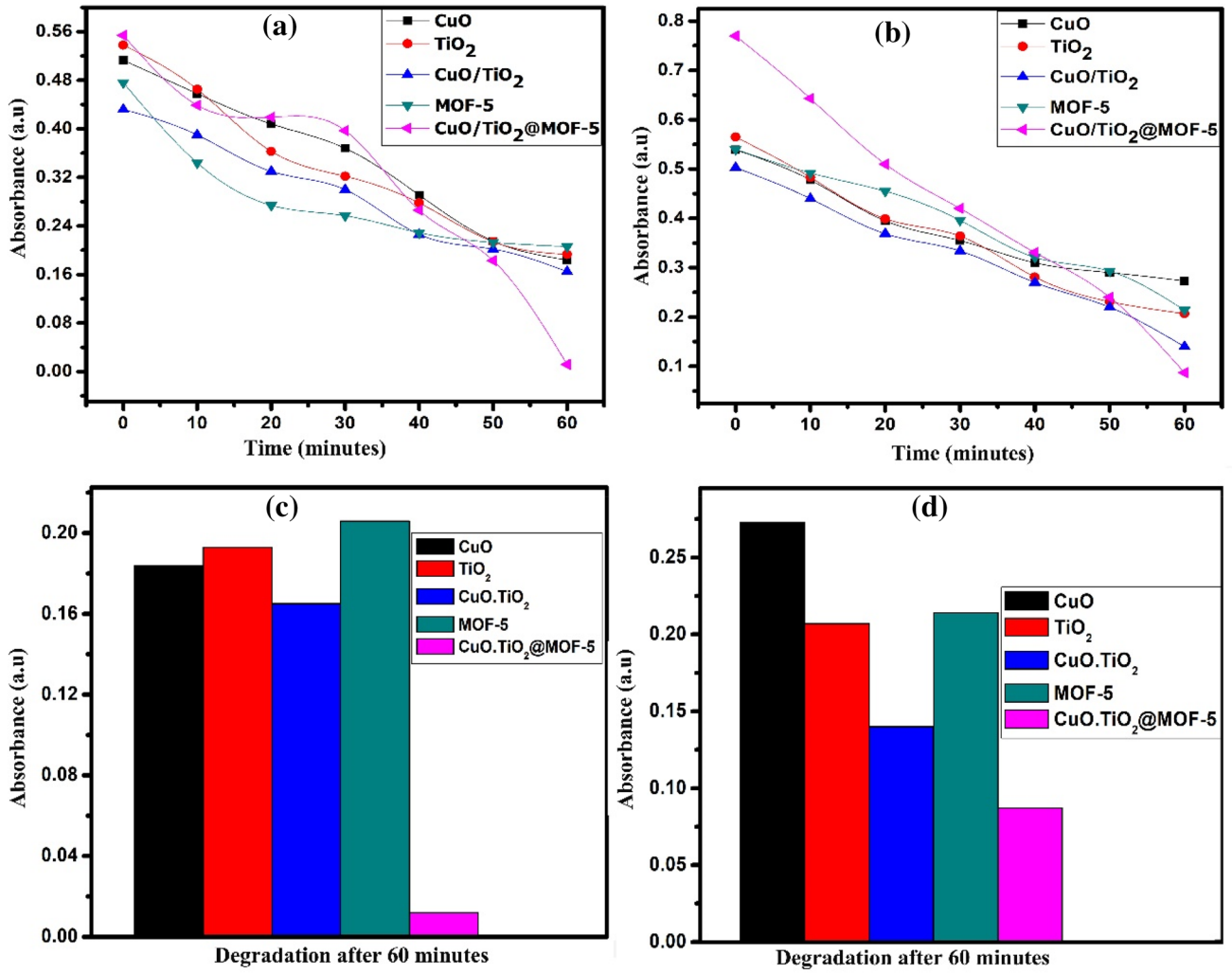

Fig. 6 **a** and **b** Photodegradation of Methylene blue (MB) and Methylene orange (MO) by different synthesized materials; **c** and **d** Photodegradation of Methylene blue (MB) and Methylene orange (MO) examine after 60 min

Table 1 Comparison of OER activity of CuO/TiO_2@MOF-5/NF with other previously reported Cu-based OER catalysts

Catalyst	Overpotential (mV) for 10 mA cm^{-2} Current density	References
CuO nanowire	580	Angew. Chem. Int. Ed 2015,54,2073
$Cu(OH)_2$	430	ChemSusChem 2016,9, 2069
$Cu(OH)_2$-CuO	417	Electrochemica Acta, 2015, 163,102.
Cu oxide	370	Angew. Chem. Int. Ed 2017,56,4792
CuO/CF	430	J.Phys.Chem.C 2017,121,25875
CuO/TiO_2@MOF-5/NF	263	This work

nanoparticles of CuO and TiO_2 do not effectively photodegrade MB and MO but after the formation of CuO/TiO_2 composite, effective photodegradation is observed. However, after the incorporation of CuO/TiO_2 composite into MOF-5, CuO/TiO_2@MOF-5 shows better photocatalytic activity as compared to individual CuO, TiO_2, MOF-5 and CuO/TiO_2 composite due to decrease of electron-hole pair recombination and increase of charge separation. It can also be observed form Fig. 7c and d that after 60 min CuO/TiO_2@MOF-5 shows minimum absorption of 0.012 and 0.087 as compared to all other synthesized samples CuO (0.184, 0.273), TiO_2 (0.193, 0.207), CuO/TiO_2 (0.165, 0.140) and

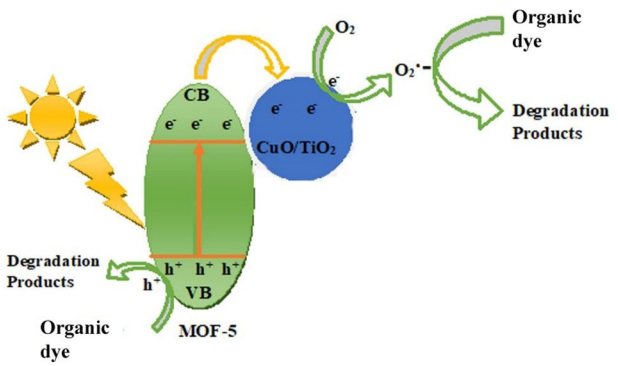

Fig. 7 Schematic representation of proposed photocatalytic mechanism for degradation of Methylene blue by CuO/TiO_2@MOF-5 in the presence of visible light

MOF-5 (0.206, 0.214), respectively for methylene blue (MB) and methyl orange (MO). It indicates that MB and MO have been successfully degraded by the synthesized samples in the presence of visible light and maximum activity has been observed by CuO/TiO_2@MOF-5.

4.3 Proposed Possible Mechanism of Photodegradation of Organic Dyes:

The possible mechanism for photocatalytic degradation of Methylene blue is as follows. The schematic representation of Possible Mechanism of Photodegradation of Organic Dyes by synthesized samples is shown by Fig. 6.

$$CuO/TiO_2@MOF\text{-}5 + h\nu \rightarrow CuO/TiO_2@MOF-5\left(h^+ + e^-\right) \quad (5)$$

$$O_2 + e^- \rightarrow O_2^{\cdot-} \quad (6)$$

$$\text{Methylene Blue/methyl orange} + O_2^{\cdot-} \rightarrow \rightarrow \rightarrow \text{degradation products} \quad (7)$$

$$\text{Methylene Blue/methyl orange} + h^+ \rightarrow \rightarrow \rightarrow \text{degradation products} \quad (8)$$

Depending upon above discussions, it is proposed that upon irradiation of visible light a number of photoexcited electrons are transferred from valence band (VB) to conduction band (CB) of MOF-5 leaving behind the positive hole (h^+) in valence band (VB). The photoexcited electrons are further transferred from CB of MOF-5 to CuO/TiO_2 and oxidized the oxygen molecules into $O_2^{\bullet-}$radicals. These $O_2^{\bullet-}$ radicals directly participate in the degradation of methylene blue and methyl orange. On the other side, positive hole (h^+) in the valance band also participates in the degradation of methylene blue as well as methyl orange.

5 Conclusions

In this reported article, highly efficient and stable catalyst CuO/TiO_2@MOF-5/NF has been synthesized by in-situ incorporation of pre-synthesized precursors into MOF-5. It has been observed that incorporation of precursors has increased the charge separation and catalytic activity of CuO/TiO_2@MOF-5 due to hetro-junction formation as compared to all other synthesized samples. The synthesized samples have been used for the study of photodegradation and electrochemical studies. Results indicate that CuO/TiO_2@MOF-5/NF has better ability for photodegradation of methylene blue as well as photoelectrochemical OER activity as compared to all other synthesized samples.

Acknowledgements Author acknowledges Higher Education Commission (HEC) of Pakistan and Institute of Chemical Sciences, Bahauddin Zakariya University, Pakistan for providing lab facilities to carry out this research work as well as Dr. Muhammad Athar for his nice suggestion and supervisions.

Compliance with Ethical Standards

Conflict of Interest Authors declare no conflict of interest.

References

1. M. Fiaz, M. Athar, JOM. 1–7 (2019)
2. P.W. Menezes, A. Indra, C. Das, C. Walter, C. Geobel, V. Gutkin, D. Schmeiber, M. Driess, ACS Catal. **7**, 103–109 (2017)
3. Y. Jiao, Y. Zhang, M.T. Jaroniec, S.Z. Qiao, Chem.Soc. Rev. **44**, 2060–2086 (2015)
4. S.H. Ye, Z.X. Shi, J.X. Feng, Y.X. Tong, G.R. Li, Angew. Chem. Int. Ed. **57**, 2672–2676 (2018)
5. K.L. Materna, B. Rudshteyn, B.J. Brennan, M.H. Kane, A.J. Bloomfield, D.L. Huang, D.Y. Shopov, V.S. Batista, Adv. Energy Mater. **4**, 1701475 (2017)
6. Y. Zeng, R. Hao, B. Xing, Y. Hou, Z. Xu, Chem. Commun. **46**, 3920–3922 (2010)
7. M. Li, T. Liu, X. Bo, M. Zhou, L. Guo, S. Guo, Nano Energy **33**, 221–228 (2017)
8. S. Peng, L. Li, X. Han, W. Sun, M. Srinivasan, S.G. Mhaisalkar, F. Cheng, Q. Yan, J. Chen, S. Ramakrishna, Angew. Chem. In. Ed. **126**, 12802–12807 (2014)
9. C. Xia, Q. Jiang, C. Zhang, G. Cui, Coord. Chem. Rev. **257**, 1946–1956 (2013)
10. C. Wang, H.Y. Li, G.L. Guo, P. Wang, Transit. Metal Chem. **38**, 275–282 (2013)
11. J. Lee, O.K. Farha, J. Roberts, K.A. Scheidt, S.T. Nguyen, J.T. Hupp, Chem. Soc. Rev. **38**, 1450–1459 (2009)
12. J.R. Li, J. Yu, W. Lu, L.B. Sun, J. Sculley, P.B. Balbuena, H.C. Zhou, Nat. Commun. **4**, 1538 (2013)
13. R.J. Kuppler, D.J. Timmons, Q.R. Fang, J.R. Li, T.A. Makal, M.D. Young, D. Yuan, D. Zhao, W. Zhuang, H.C. Zhou, Coord. Chem. Rev. **253**, 3042–3066 (2009)
14. K. Sumida, D.L. Rogow, J.A. Mason, T.M. McDonald, E.D. Bloch, Z.R. Herm, T.H. Bae, J.R. Long, Chem. Rev. **112**, 724–781 (2011)

15. H.C. Zhou, J.R. Long, O.M. Yaghi, Chem. Rev. **112**, 673–674 (2012)
16. H.B. Wu, X.W. Lou, Sci. Adv. **3**, 9252 (2017)
17. M. Alvaro, E. Carbonell, B. Ferrer, F.X. LlabresiXamena, H. Garcia, Chem-Eur. J. **13**, 5106–5112 (2007)
18. L.R. Hou, C.Z. Yuan, Y. Peng, J. Hazard. Mater. **139**, 310–315 (2007)
19. A.H. Jawad, A.F. Alkarkhi, N.S.A. Mubarak, Desalin. Water Treat. **2014**, 1–12 (2014)
20. A.N. Ejhieh, M.K. Shamsabadi, Appl. Catal. A **477**, 83–92 (2014)
21. Y. Fang, Y.R. Wang, G. Jiang, H. Jin, Y. Wang, X. Sun, S. Wang, T. Wang, Bull. Mater. Sci. **35**, 495–499 (2012)
22. J.M. Kshirsager, R. Shrivastava, P.S. Adwani, Thermal Sci. **2**, 233–242 (2017)
23. W. Li, T. Zeng, PLoS ONE **6**, 21082 (2011)
24. M. Fiaz, M. Kashif, S. Majeed, M.N. Ashiq, M. Athar, M.A. Farid, ChemistrySelect **4**, 6996–7002 (2019)
25. J.H. Shah, M. Fiaz, M. Athar, J. Ali, M. Rubab, R. Mahmood, S.U. U. Jamil, R. Djellabi, Environmental Technology, 2019
26. M. Fiaz, M. Athar, ChemistrySelect, 2019, 4, 8508–8515
27. C.M. Magdalane, K. Kaviyarasu, N. Matinise, N. Mayedwa, N. Mongwaketsi, D. Letsholathebe, G.T. Mola, N.A. Al-Dhabi, M.V. Arasu, M. Henini, J. Kennedy, M. Maaza, B. Jeyaraj, S. Afr. J. Chem. Eng. **26**, 49–60 (2018)
28. C.M. Magdalane, K. Kaviyarasu, G.M. Priyadharisni, A.K.H. Bashir, N. Mayedwa, N. Matinise, A.B. Isaev, N.A. Al-Dhabi, M.V. Arasu, S. Arokiyaraj, J. Kennedy, M. Maaza, J. Mater. Res. Technol. **8**(3), 2898–2909 (2019)

Affiliations

Abdul Jabbar[1] · Muhammad Fiaz[1] · Sonia Rani[1] · Muhammad Naeem Ashiq[1] · Muhammad Athar[1]

✉ Muhammad Athar
athar.qr@bzu.edu.pk

[1] Institute of Chemical Sciences, Bahauddin Zakariya University, Multan 60800, Pakistan